PHYSICAL REVIEW B VOLUME 18, NUMBER 10 15 NOVEMBER, 1978

Electron-phonon scattering and high-field transport in n-type Si

M. H. Jørgensen
Physics Laboratory III, The Technical University of Denmark, DK 2800 Lyngby, Denmark
(Received 1 July 1977)

The transport problem for warm and hot electrons in silicon is formulated using a simple, nonparabolic band model. The electronic distribution function is written in terms of an extended diffusion approximation which allows for a certain amount of "streaming" of the distribution in momentum space. The solution of the Boltzmann equation is reduced to the solution of a coupled set of ordinary second-order differential equations which are well suited for iterative numerical techniques. By comparing experimental and numerical data we can assign realistic values to electron-phonon coupling constants and a good overall fit is obtained for several types of experiment.

I. INTRODUCTION

Although silicon crystals have been extensively studied for many years, our detailed understanding of certain basic processes such as electron-phonon scattering is not completely satisfying. In particular, one may recall the controversy about the relative importance of f- and g-type intervalley scattering and the uncertainty about which phonon modes are actually responsible for such processes.

The theoretical results available are mainly concerned with the selection rules for phonon-induced intervalley transitions. The relative importance of the different "allowed" phonons must be determined from experimental data.

The possible experiments which could provide such information may be classified according to the following scheme: (a) optical experiments, (b) simple transport experiments (without quantizing magnetic fields) and (c) magnetophonon resonance (MPR) experiments. In the cases (a) and (c), the relevant phonon energies are connected with the experimental data in a reasonably straightforward way, although the interpretation is not entirely unambiguous.

The largest amount of experimental evidence originates, however, from simple transport experiments where the electronic drift velocity (or the current) is measured for different values of applied field, pressure, temperature, doping level, etc. Here, the problem is how to make the best overall fit between a representative set of experimental data and the numerical results obtained from a detailed theoretical model which includes all the possible types of phonon scattering. A necessary prerequisite for this type of analysis is a general method of solving the nonlinear Boltzmann equation arising in the warm- and hot-electron cases. We should like to stress the point that warm-electron effects (i.e., small nonlinearities observed at lower electric fields) may provide valuable information about the detailed nature of the scattering mechanisms. Therefore, when testing phonon scattering models by comparing the saturated I-V curves from high-field experiments with numerical calculations, one should include a check on the warm-electron parameters. (A simultaneous fit to both types of experiment is by no means trivial.) It follows that numerical methods which allow calculation of warm- as well as hot-electron parameters are to be preferred.

Because of the interest in studying f-type scattering (between perpendicular valleys) in silicon it is natural to emphasize experiments where valley repopulation can be observed. This type of experiment, however, must be analysed using a theory which takes into account a possible scattering anisotropy since this may influence the valley repopulation in much the same way as the effective-mass anisotropy in a single valley (although the latter is generally larger than the scattering anisotropy).

In the present work, the main emphasis is placed upon obtaining a reasonable fit to a set of experimental warm- and hot-electron results obtained in this laboratory over nearly a decade. The primary tool is a computer program which solves the Boltzmann equation for the many-valley conduction band of n-Si, taking into account f and g transitions between the valleys as well as the anisotropic scattering by long-wavelength acoustic phonons and ionized impurities. Energy relaxation due to acoustic-phonon scattering is included for the sake of completeness (although generally not very important). The calculations are based on a theoretical model which seems to be compatible with the results from MPR experiments (but not with the theoretical selection rules).

II. THEORETICAL MODEL

The model assumes a conduction band with six equivalent minima located on the ⟨100⟩ axes in re-

ciprocal space. We assume that the total energy ϵ of an electron with wave vector $\vec{k}$ close to the minimum $\vec{k}_\nu^0$ of the νth valley) will satisfy the equation

$$(\epsilon-\epsilon_\nu^0)\left[1+\frac{(\epsilon-\epsilon_\nu^0)}{\epsilon_G}\right]=\tfrac{1}{2}\hbar^2(\vec{k}-\vec{k}_\nu^0)\cdot\vec{\vec{m}}_\nu^{-1}\cdot(\vec{k}-\vec{k}_\nu^0)\,. \quad (1)$$

Here, ϵ_ν^0 denotes the minimum energy of the valley. (A uniaxial pressure may cause different valleys to have different minimum energies.) The effective-mass tensor $\vec{\vec{m}}_\nu$ describes the valley around the νth minimum. The $\vec{\vec{m}}_\nu$ tensor (which is assumed to be independent of ϵ) has transverse and longitudinal eigenvalues $m_\perp$ and $m_\parallel$. A possible nonparabolicity of the conduction band is taken into account in a phenomenological way by assuming a band structure which is generally hyperbolic rather than parabolic. The parameter ϵ_G indicates the energy threshold above which significant deviations from the parabolic shape will occur. (Obviously, the limit $\epsilon_G\to\infty$ corresponds to the parabolic case.)

In the following, we shall use (instead of $\vec{k}$) the transformed wave vector[1]

$$\vec{k}=\hbar(2\vec{\vec{m}}_\nu)^{-1/2}\cdot(\vec{k}-\vec{k}_\nu^0)\,. \quad (2)$$

This transformation simplifies Eq. (1) which may now be written

$$(\epsilon-\epsilon_\nu^0)[1+(\epsilon-\epsilon_\nu^0)/\epsilon_G]=K^2\,. \quad (1a)$$

The quantity of basic interest is the electronic distribution $f_\nu(\vec{K})$. We shall employ what may be called an extended diffusion approximation, writing $f_\nu(\vec{K})$ in the form

$$f_\nu(\vec{K})\simeq F_\nu(K)+\vec{K}\cdot\vec{G}_\nu(K)+\vec{K}\cdot\vec{\vec{H}}_\nu(K)\cdot\vec{K}\,. \quad (3)$$

In the simple diffusion approximation only the terms with $F_\nu(K)$ and $\vec{G}_\nu(K)$ are considered. The additional term with $\vec{\vec{H}}_\nu(K)$ describes the possible "streaming" of the distribution in $\vec{K}$-space. Without loss of generality, $\vec{\vec{H}}_\nu$ may be taken as a symmetric tensor with $\mathrm{tr}(\vec{\vec{H}}_\nu)=0$.

The stationary distribution in the νth valley can be determined from the Boltzmann equation

$$-\dot{\vec{K}}_\nu\cdot\nabla_K f_\nu(\vec{K})+\left(\frac{\partial f_\nu}{\partial t}\right)_{\text{scatt}}=0\,. \quad (4)$$

Here the normalized field for the νth valley is defined by

$$\dot{\vec{K}}_\nu=-e(2\vec{\vec{m}}_\nu)^{-1/2}\cdot\vec{E}\,, \quad (5)$$

where $\vec{E}$ is the external electric field. By inserting (3) into (4) and separating terms with different symmetry properties we obtain the following set of equations:

$$\left(\frac{\partial F_\nu}{\partial t}\right)_{\text{scatt}}=\frac{1}{3K^2}\frac{\partial}{\partial K}\left[K^3\dot{\vec{K}}_\nu\cdot\vec{G}_\nu(K)\right], \quad (6)$$

$$\left(\frac{\partial\vec{G}_\nu}{\partial t}\right)_{\text{scatt}}=\frac{1}{K}\dot{\vec{K}}_\nu\frac{\partial F_\nu}{\partial K}+\frac{2}{5K^4}\frac{\partial}{\partial K}\left[K^5\dot{\vec{K}}_\nu\cdot\vec{\vec{H}}_\nu(K)\right], \quad (7)$$

$$\left(\frac{\partial\vec{\vec{H}}_\nu}{\partial t}\right)_{\text{scatt}}=\frac{1}{K}\frac{\partial}{\partial K}\left[\tfrac{1}{2}(\dot{\vec{K}}_\nu\vec{G}_\nu(K)+\vec{G}_\nu(K)\dot{\vec{K}}_\nu)-\tfrac{1}{3}\vec{\vec{1}}\,\vec{G}_\nu\cdot\dot{\vec{K}}_\nu\right], \quad (8)$$

(The unit tensor is denoted by $\vec{\vec{1}}$.)

It may be noted that the disturbance from the applied field will couple F_ν and $\vec{G}_\nu$ together as well as $\vec{G}_\nu$ and $\vec{\vec{H}}_\nu$. However, there is no field-coupling between F_ν and $\vec{\vec{H}}_\nu$.

A conduction electron will travel with the group velocity $\vec{v}=(1/\hbar)\nabla_k\epsilon$. Using (1) and (2) we obtain

$$\vec{v}(\vec{K})=(\tfrac{1}{2}\vec{\vec{m}}_\nu)^{-1/2}\cdot\vec{K}/\zeta(K)\,, \quad (9)$$

where

$$\zeta(K)=\frac{\partial(K^2)}{\partial\epsilon}=1+\frac{2(\epsilon-\epsilon_\nu^0)}{\epsilon_G}=\left(1+\frac{4K^2}{\epsilon_G}\right)^{1/2}. \quad (10)$$

The quantity ζ appears here as a nonparabolocity correction factor in the velocity equation. Later, the same factor will appear in all the scattering terms where it is introduced, in general, via the energy-conserving δ function in the "golden rule" scattering probabilities.

Given the electronic distribution (the $F_\nu(K)$ and $\vec{G}_\nu(K)$ functions) we can evaluate the average drift velocity:

$$\vec{v}_d=\frac{1}{3}\frac{\sum_\nu(\tfrac{1}{2}\vec{\vec{m}}_\nu)^{-1/2}\cdot\int_0^\infty K^4[\vec{G}(K)/\zeta(K)]\,dK}{\sum_\nu\int_0^\infty F_\nu(K)K^2\,dK}\,. \quad (11)$$

In the limit of zero electric field the electronic drift mobility can be calculated in a straightforward way from Eqs. (7) and (11) because $F_\nu(K)$ may be approximated by the thermal equilibrium distribution and $\vec{\vec{H}}_\nu(K)$ by zero.

At higher fields the coupled system of Eqs. (6)–(8) must be solved numerically. An iterative method of solution is reviewed in Appendix A.

To specify the model completely we must now deal with the evaluation of the scattering terms on the left hand side of Eqs. (6)–(8).

To simplify the numerical calculations we shall use relaxation-time approximations as far as possible. Since all the relevant scattering mechanisms are either isotropic or (almost) energy conserving we may introduce a momentum relaxation-time tensor as pointed out by Herring and Vogt.[1] Then the $\vec{G}_\nu$ term takes the form

$$\left(\frac{\partial\vec{G}_\nu}{\partial t}\right)_{\text{scatt}}=-\vec{\vec{\tau}}_\nu^{-1}\cdot\vec{G}_\nu(K)\,, \quad (12)$$

where $\vec{\vec{\tau}}(K)$ has the symmetry of the valley with transverse and longitudinal eigenvalues $\tau_{\nu\perp}(K)$ and $\tau_{\nu\parallel}(K)$. (Unless the valleys are displaced by a uniaxial pressure, the $\tau_\perp$ and $\tau_\parallel$ functions are the

same for all valleys.)

In the case of n-Si the streaming correction as described by $\tilde{\tilde{H}}_\nu$ is relatively small. Therefore, we shall avoid a more elaborate relaxation time formalism and simply put:

$$\left(\frac{\partial \tilde{\tilde{H}}_\nu}{\partial t}\right)_{\text{scatt}} \simeq \frac{-1}{\tau_{\nu\perp}(K)}\,\tilde{\tilde{H}}_\nu(K)\,. \tag{13}$$

Thus the "streaming relaxation time" (in principle a fourth-order tensor) is assumed to be scalar and is furthermore approximated by the transverse momentum relaxation time $\tau_{\nu\perp}(K)$. (This becomes a very good approximation in the hot-electron case where isotropic scattering mechanisms are dominating.) The reciprocal relaxation times may be written (with $\lambda = \perp$ or $\|$)

$$\frac{1}{\tau_{\nu\lambda}(K)} = \zeta(K)\left[W_{ac\lambda}K + \frac{W_i}{K^3}\,a_\lambda\left(\ln[1+(b_\lambda QK^2)^2] - \frac{c_\lambda}{1+(d_\lambda/QK^2)^2}\right)\right] + \sum_{\mu\neq\nu}\sum_m W_{\nu\mu}^{(m)}\left[n_{\nu\mu}^{(m)}K_+\zeta(K_+) + (n_{\nu\mu}^{(m)}+1)K_-\zeta(K_-)\right]. \tag{14}$$

Here, $W_{ac\lambda}$ is an acoustic-phonon coupling constant which depends on the lattice temperature T and the elastic coefficients c_{ij}:

$$W_{ac\lambda} = \frac{60\pi^3\sqrt{2}\,m_\perp m_\|^{1/2}kT}{h^4(3c_{11}+2c_{12}+4c_{44})}\,\Xi_\lambda^2\,. \tag{15}$$

The effective deformation potentials $\Xi_\perp$ and $\Xi_\|$ are defined in Appendix B as simple functions of Ξ_d and Ξ_u and the "electrostatic" coefficients[2] C_1 and C_2.

Scattering by ionized impurities is characterized by the constant[3]

$$W_i = \frac{3\pi e^4 m_\perp N_i}{2\sqrt{2}\,(4\pi\epsilon_0\kappa)^2 m_\|^{1/2}} \tag{16}$$

and a screening parameter

$$Q = \frac{(4\pi\epsilon_0\kappa)2\pi m_\| kT}{e^2h^2N_e}\,, \tag{17}$$

where N_i and N_e are the concentrations of ionized impurities and conduction electrons. The dimensionless coefficients $a_\perp, b_\perp, \ldots, d_\|$ are given in Appendix B.

$W_{\nu\mu}^{(m)}$ denotes an intervalley phonon coupling constant for transitions between valleys No. ν and μ by phonons of type m. $\hbar\omega_{\nu\mu}^{(m)}$ and $n_{\nu\mu}^{(m)}$ are the corresponding phonon energy and occupation number. In terms of the deformation potential $D_{\nu\mu}^{(m)}$ we have

$$W_{\nu\mu}^{(m)} = \frac{2\pi\sqrt{2}\,m_\perp m_\|^{1/2}}{h^2\rho\hbar\omega_{\nu\mu}^{(m)}}\,(D_\mu^{(m)})^2 \tag{18}$$

(ρ is the specific weight of the crystal). The quantities $K_\pm$ are defined by

$$K_\pm = \{K^2 + \Delta\epsilon_\pm[\,\zeta(K) + \Delta\epsilon_\pm/\epsilon_G\,]\}^{1/2} \tag{19}$$

with ,

$$\Delta\epsilon_\pm = \pm\hbar\omega_{\nu\mu}^{(m)} + \epsilon_\nu^0 - \epsilon_\mu^0\,. \tag{19a}$$

It is understood that $K_\pm = 0$ when a negative argument appears under the square-root sign in Eq. (19). When $\epsilon_G \to \infty$ (parabolic bands), Eq. (19) yields $K_\pm = [K^2 + \Delta\epsilon_\pm]^{1/2}$.

The spherically symmetric part of the distribution is influenced by scattering processes in a more complicated way which makes simple relaxation-time approximations impossible. The dominating contribution to $(\partial F_\nu/\partial t)_{\text{scatt}}$ comes from intervalley scattering. Also, acoustic energy relaxation has been included in the general expression. The energy conserving impurity scattering does not influence $F_\nu(K)$ directly since we neglect impurity induced intervalley transitions. The total expression then becomes[4]:

$$\left(\frac{\partial F_\nu}{\partial t}\right)_{\text{scatt}} = W_{ac\epsilon}\,\frac{kT}{2K^2}\,\frac{d}{dK}\left[[K^2\zeta(K)]^2\left(\frac{dF_\nu}{d\epsilon} + \frac{F_\nu(K)}{kT}\right)\right] + \sum_{\mu\neq\nu}\sum_m W_{\mu\nu}^{(m)}\left[[F_\mu(K_+)(n_{\mu\nu}^{(m)}+1) - F_\nu(K)n_{\mu\nu}^{(m)}]\,K_+\zeta(K_+)\right.$$
$$\left. + [F_\mu(K_-)n_{\mu\nu}^{(m)} - F_\nu(K)(n_{\mu\nu}^{(m)}+1)]K_-\zeta(K_-)\right] \tag{20}$$

[with symbols $K_\pm$ as defined by (19)]. The constants $W_{\mu\nu}^{(m)}$ have already been defined. The acoustic energy relaxation parameter $W_{ac\epsilon}$ is defined by[4]

$$W_{ac\epsilon} = \frac{32\sqrt{2}\,\pi^3 m_\perp^2 m_\|^{1/2}}{h^4\rho}\,\Xi_0^2\,. \tag{21}$$

The effective deformation potential Ξ_0 for acoustic energy relaxation may be calculated by methods very similar to those employed in Ref. 2 for the calculation of $\Xi_\perp$ and $\Xi_\|$. The numerical coefficients relating Ξ_0 to Ξ_u, Ξ_d, C_1, and C_2 are given in Appendix B.

It is seen that Eq. (20) describes the energy-exchange between the electron gas and the phonons as well as the energy- and electron-exchange between different valleys.

III. ACOUSTIC PHONON PARAMETERS

The choice of acoustic scattering parameters (Ξ_u, Ξ_d, C_1, and C_2) must be consistent with the results from a number of different experiments and theoretical calculations.

Balslev's piezo-optical experiments[5] indicate that Ξ_u must be close to 8.6 eV. Several measurements of the electronic mobility in pure crystals[6,7] at lower temperatures (where contributions from ionized impurities and intervalley phonons may be neglected) show that the acoustic-phonon limited mobility at 77 K lies between 25 000 and 27 000 cm^2/V sec. Also the acoustic scattering anisotropy is important. Recent piezoresistance data[8] indicate that $(\tau_{\parallel}/\tau_{\perp})_{ac} \simeq 0.81$. Finally, we may employ[2] a theoretical result by Pindor[9] who found $C_{qua} = \frac{5}{2}C_1 + \frac{3}{2}C_2) \simeq 2.7$ eV.

From these data we have obtained a solution for Ξ_d, C_1 and C_2. All the parameters relevant for acoustic scattering are summarized in Table I.

TABLE I. Acoustic scattering parameters for n-Si.

Ξ_u	8.60	eV
Ξ_d	−0.30	eV
C_1	3.35	eV
C_2	−3.78	eV
$m_\perp/m_0$	0.1905	
$m_\parallel/m_0$	0.9163	
C_{11}	1.657×10^{11}	N/m^2
C_{12}	0.639×10^{11}	N/m^2
C_{44}	0.796×10^{11}	N/m^2
ρ	2420	kg/m^3

IV. INTERVALLEY SCATTERING AND NONPARABOLICITY

A group-theoretical analysis of the matrix elements for electron-phonon scattering has been carried out by Streitwolf[10,11] who corrected some errors in earlier treatments.[12] Streitwolf's result is that the matrix elements of most intervalley phonons vanish due to symmetry. Only LO-type g phonons and LA- and TO-type f phonons are allowed when only zero-order processes are considered. Also, transitions by LO and TO intravalley phonons (with zero wave vector) are prohibited.

From the well-known phonon spectrum of silicon[13] we obtain the following energies for the allowed intervalley phonons:

$$\hbar\omega_g(\mathrm{LO}) \simeq 62 \text{ meV},$$

$$\hbar\omega_f(\mathrm{TO}) \simeq 59 \text{ meV},$$

$$\hbar\omega_f(\mathrm{LA}) \simeq 47 \text{ meV}.$$

The values are determined by assuming that the distance from $k = 0$ to the valley-minima is 85% of the distance to the Brillouin-zone boundary (in consistency with Streitwolf's assumption that the intervalley phonon transitions are Umklapp processes).

The phonon energies obtained by this procedure are in very good agreement with those obtained by MPR experiments.[14] These experiments, however, also seem to prove that there is a quite significant coupling between electrons in n-Si and a 12-meV TA-type g phonon which should not be allowed, according to group theory. This evidence is supported by the experience during the progress of the present work: It seems quite difficult to obtain a good fit between numerical calculations and experimental data from simple transport experiments unless a significant contribution from a g phonon of rather low energy is allowed.

By Fourier-analyzing different MPR spectra for n-Si Eaves *et al.*[14] have shown that in addition to the three "allowed" phonons and the rather dominant "forbidden" 12-meV phonon also an LA-type g phonon (with energy 19 meV) may be active. The 12-meV phonon was, however, the only "forbidden" phonon which showed up at ali sample orientations.

In the numerical calculations to be presented here it has turned out that by using two f-phonons (59 and 47 meV) and two g phonons (62 and 12 meV) we may obtain a reasonable fit to simple transport data (hot- and warm-electron data and mobility versus temperature).

The intervalley phonon deformation potentials [the $D_{\nu\mu}^{(n)}$ constants in Eq. (18)] have been used as fitting parameters while fixed acoustic phonon parameters have been used (corresponding to the data given in Table I).

The electronic mobility in pure n-Si is assumed to be 1450 cm^2/Vsec at 300 K.[7] Since the acoustic-phonon limited mobility (calculated from a parabolic model) is 3500 cm^2/V sec at 300 K we can estimate the combined effect of nonparabolicity and scattering by high-energy phonons.

A distinction between f- and g-phonon contributions can be made from piezoresistance data. Consider two experiments with uniaxial pressure applied in [001] and [011] directions, respectively. In both cases the electric field is applied along [100]. In the saturation limit all electrons are concentrated in the [001] valley (with [001] pressure) or in the [010] and [001] valleys (with [011] pressure) and in either case the transverse mobility is measured since the electric field is perpendicular to populated valleys. In the first case it is obvi-

ous that f scattering has been entirely eliminated since only one set of valleys (along [001]) is populated. In the second case, however, only 50% of the original f scattering is eliminated since transitions between [010] and [001] valleys may still take place. The saturation mobility should be the same in the two cases if f scattering were negligible. By comparing experimental mobility versus pressure curves[15] with numerical calculations we may ensure that the relative magnitude of f scattering as compared to other scattering mechanisms is essentially correct.

Any set of $D_{\nu\mu}^{(m)}$ values to be used as fitting parameters in hot- or warm-electron calculations has been tested as indicated above: (i) the room temperature mobility must be close to 1450 cm^2/V sec and (ii) the relative contribution from f scattering must be consistent with piezoresistance data at 300 K. The effect of nonparabolicity is easy to explain in qualitative terms: (a) As shown by Eqs. (14) and (20) the efficiency of all scattering mechanisms is increased by the factor $\zeta(K)$ which becomes significant unless $K^2 \ll \epsilon_G$. (b) As shown by Eqs. (9)–(11) $\zeta(K)$ will also appear as a limiting factor in the calculation of the electronic drift velocity. Therefore a nonparabolicity will cause a stronger current saturation at very high electric fields and electron temperatures.

It turns out that calculations based on a parabolic model for n-Si will never predict current saturation at high lattice temperatures. Experimental I-V curves, however, clearly exhibit current saturation, also at lattice temperatures of 300–480 K.[16,17] This has already been discussed by Jacoboni *et al.*[18] who showed (by Monte Carlo calculations) that a much improved fit was obtained by using a hyperbolic band model with $\epsilon_G = 2$ eV.

This result was confirmed in our calculations and we have adopted the value $\epsilon_G = 2$ eV in the calculations to be discussed in the following. With $\epsilon_G = 2$ eV one obtains from Eq. (1) that the transverse cyclotron mass should increase by 0.3% per meV of electronic energy. This seems to be in fair agreement with recent experimental data.[19]

V. COMPARISON WITH EXPERIMENTAL DATA

The determination of the "best" $D_{\nu\mu}^{(m)}$ values was mainly carried out by fitting the numerical calculations to two experimental curves: (a) β vs. p (at $T = 77$ K) with $\vec{E} \parallel [100]$ and uniaxial pressure applied along [100]. (b) β vs. T (for $T = 77$–250 K) with $\vec{E} \parallel [111]$. (The warm-electron coefficient β is defined by $v_d(E) \simeq \mu(0)(1 + E^2\beta)E$ at low electric fields[3]). The phonon parameters obtained in this way are then tested by comparison between theoretical results and typical experimental hot-electron data.

TABLE II. Intervalley scattering parameters for n-Si.

$D_{\nu\mu}^{(m)}$ (eV/m)	$\hbar\omega_{\nu\mu}^{(m)}$ (meV)	Phonon mode	Type of scattering
$D_{f59} = 2 \times 10^{10}$	59	TO	f
$D_{f47} = 4.3 \times 10^{10}$	47	LA	f
$D_{g62} = 7.5 \times 10^{10}$	62	LO	g
$D_{g12} = 0.65 \times 10^{10}$	12	TA	g

The intervalley phonon parameters which give the best overall fit to the experimental curves are shown in Table II. In the following these data are always referred to as DATA I.

It turns out that the distribution of scattering power between the "allowed" 62 meV and the "forbidden" 12 meV g phonon has a strong influence on the value of β when the electric field is parallel to [100]. When $\vec{E} \parallel [111]$, however, this influence on β is minimal. This point is illustrated by Fig. 1 where $\beta_{[100]}$ is shown as a function of applied uniaxial pressure at 77 K,[20] and Fig. 2 which shows $\beta_{[111]}$ versus temperature[3] (no stress).

Three sets of theoretical points are shown, labeled DATA I, II, and III. The DATA II curves

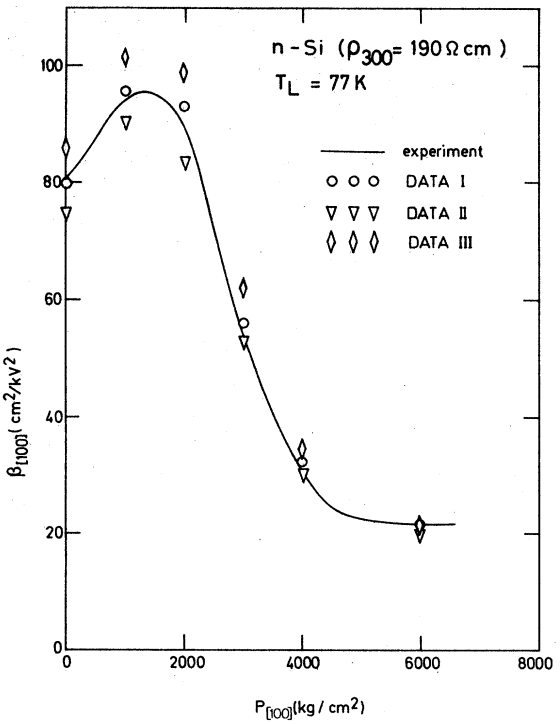

FIG. 1. Warm-electron coefficient β vs. uniaxial pressure p at 77 K. Electric field and pressure are applied along [100]. (The curve is experimental and the points are calculated.)

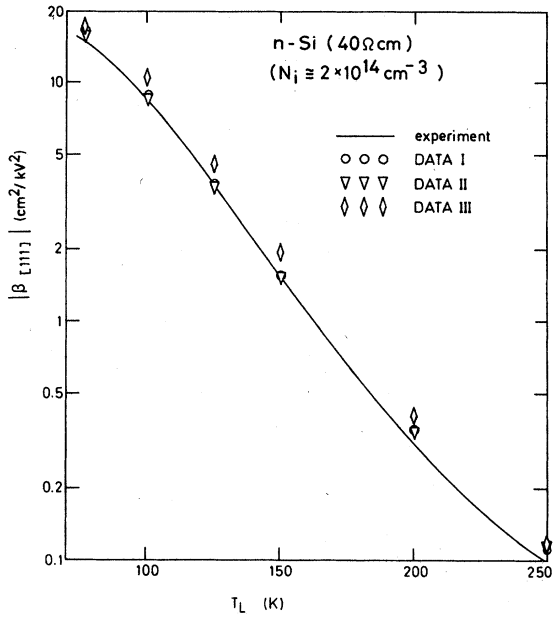

FIG. 2. Warm-electron coefficient β vs temperature. Electric field is applied along [111]. (The curve is experimental and the points are calculated.)

were calculated with a slightly higher value of D_{g12} and a correspondingly lower value of D_{g62}: $D_{g12}=0.7\times10^{10}$ eV/m and $D_{g62}=7\times10^{10}$ eV/m (otherwise as DATA I).

The distribution of scattering power between the two f-type phonons is not quite as critical. This is hardly surprising since the phonon energies (59 and 47 meV) are not very different. The effect of redistributing the scattering power between the 47 and 59 meV phonons is illustrated by the DATA III points which were calculated with a higher D_{f59} value and a lower D_{f47} value: $D_{f59}=6\times10^{10}$ eV/m and $D_{f47}=2$ eV/m (otherwise as DATA I).

There is a very clear tendency for $\beta_{[100]}$ as well as $\beta_{[111]}$ to become too large when the D_{f59}/D_{f47} ratio is increased as strongly as here. It is, however, not likely that simple transport measurements can produce a very accurate determination of this ratio.

Now we turn to hot-electron experiments at 77 K. Figure 3 shows the normalized drift velocity $v_d/\mu(E=0)$ as a function of applied field along [100] and [111].

Experimental curves are averages over results obtained by Hansen[15] and Jørgensen[21] whose data are in very good agreement. It should be noted that the experiments were carried out with voltage pulses about 1 μsec long. This means that the pulse length is greater than characteristic relaxation times at this temperature. (This applies not only to momentum relaxation times but to energy relaxation times and valley repopulation time constants as well.) Therefore, a stationary electronic distribution can be assumed during the drift pulse as long as the pulse length, on the other hand, is sufficiently short to avoid heating of the crystal lattice.

There is some discrepancy between our experimental curves and those published by Canali *et al.*[22] Their curves were obtained by time-of-flight measurements with nanosecond pulses on very short samples. A comparison shows that the important "kink" on the [100] curves seems to be somewhat suppressed and shifted to higher fields in the time-

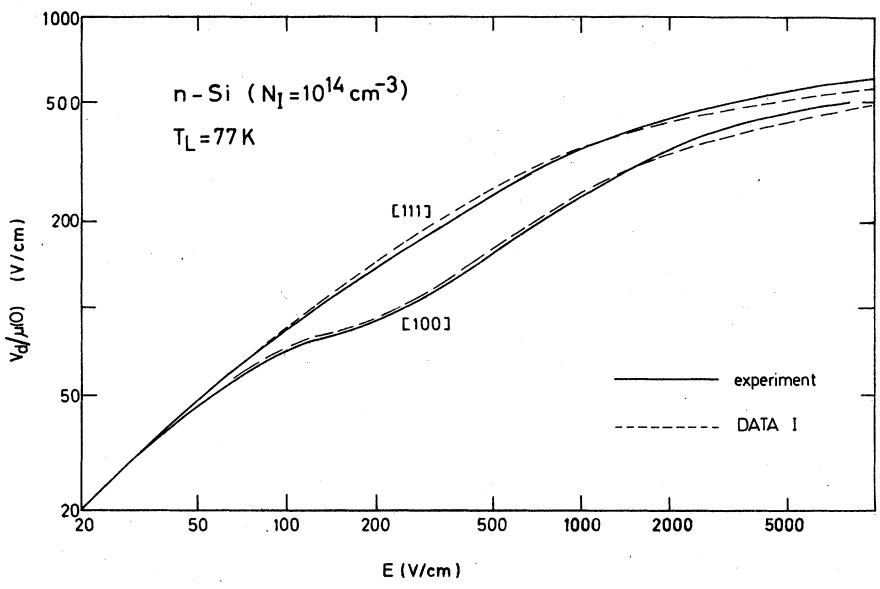

FIG. 3. Normalized drift velocity $v_d(E)/\mu(0)$ vs electric field E at 77 K. Electric field is applied along [100] and [111]. (Full lines signify experiment and broken lines signify theory.)

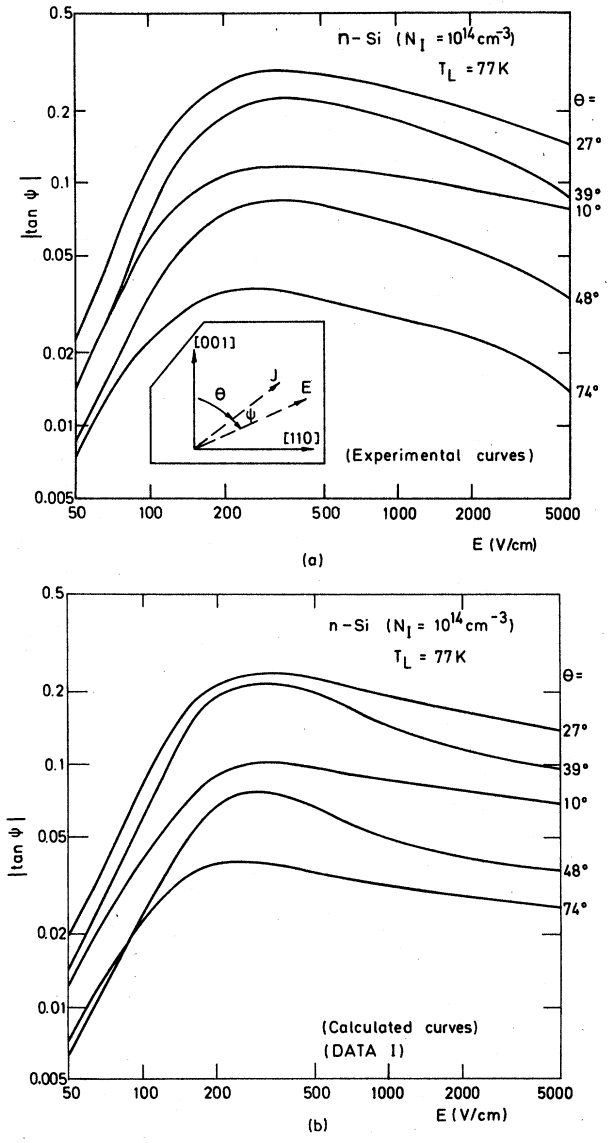

FIG. 4. (a) Experimental curves showing magnitude of the anisotropy factor $\tan\psi = E_\perp/E$ vs longitudinal electric field E at 77 K. (Angle θ defines sample orientation, see inset.) (b) Theoretical curves [otherwise as (a)].

of-flight measurements. A possible interpretation of this discrepancy may be that at 77 K and fields below 1 kV/cm typical repopulation time constants (for electron transfer from "hot" to "cold" valleys) are not short compared to the pulse length and/or the transit time in the time-of-flight experiments. If this is true the measured drift velocity does not correspond to a stationary electronic distribution. Since the numerical calculations are based on the assumption of a stationary distribution the theoretical curves should be compared with experimental I-V curves obtained by long pulses.

The theoretical DATA I curves are in good agreement with the experimental curves, and DATA II curves (not shown) will, in fact, fit the experiments equally well. DATA III curves (not shown) slightly exaggerate the "kink" around 200 V/cm but are otherwise identical with DATA I and II curves. Thus, it appears that hot-electron experiments are less sensitive to the detailed structure of electron-phonon interaction than warm-electron experiments.

Phonon scattering data derived from a comparison between Monte Carlo calculations and (short pulse) time-of-flight experiments are suggested in Ref. 22. (Similar data are found in Ref. 18, with small corrections for nonparabolicity.) They deviate from our parameters in two ways: (i) Three "forbidden" intervalley phonons of low energy are included, among those an f-type phonon and (ii) long-wavelength acoustic-phonon scattering is treated in a phenomenological way, using an isotropic scattering model.

We have performed calculation with the data of Ref. 18 in our numerical model. As expected, these calculations give a reduced warm-electron anisotropy at lower temperatures ($\beta_{[100]}$ becomes about 25% too small at 77 K). At temperatures $\geq$300 K and fields $\geq$30 kV/cm, however, the data of Ref. 18 give a slightly improved fit to the velocity saturated experimental I-V curves. The difference is too small to be conclusive and the crude band model (used in this work as well as in Ref. 18) may be inadequate at these very high fields with "electron temperatures" in excess of 2000 K.

The hot-electron anisotropy can be investigated in a more detailed way by measuring the angular deviation between the current and field directions at different electric fields (Sasaki-Shibuya effect[23]). The experimental procedure[21,23] could be characterized briefly as a "Hall-effect measurement without magnetic field and with a pulsed electric field."

Our experimental results[21] are shown in Fig. 4(a) (with an inset defining the experimental geometry). Because of symmetry[24] the anisotropy factor $|\tan\psi| = 0$ for $\theta = 0°$, 54.7°, and 90° ($\vec{J} \parallel [001]$, $\vec{J} \parallel [111]$ and $\vec{J} \parallel [110]$). Qualitative discussions of the observed effect may be found elsewhere.[25] At higher electric fields the effect is quite large, but some experimental difficulties arise because the current saturation means that the longitudinal electric field in the critical zone near the transverse potential probes is not very well defined. At low electric fields the relative magnitude of the effect becomes small and large common mode signals as well as capacitive effects will reduce the experimental accuracy.

The theoretical curves (calculated with the pre-

ferred DATA I parameters) are shown in Fig. 4(b). There is a good qualitative agreement with Fig. 4(a), considering the fact that accurate, absolute measurements of $|\tan\psi|$ are rather difficult.

VI. CONCLUSION

We have shown that several warm- and hot-electron experiments can be interpreted successfully in terms of the available information about the electron-phonon coupling in silicon. Approximate values have been assigned to some of the unknown electron-phonon coupling constants.

The experimental results seem to have an important feature in common with the results from MPR experiments: The theoretical explanation must include coupling to at least one phonon of low energy although such couplings seem forbidden by symmetry. Our calculations give full support to the conclusions reached by Jacoboni and co-workers[18] about the nonparabolicity of the conduction band, which becomes important at higher temperatures.

We have described numerical methods suitable for solving the stationary hot-electron transport problem in any nonpolar semiconductor with a many-valley conduction band. It should be mentioned that although our method was initially aimed at the stationary problem, it is possible to calculate (by repeated iterations) a set of coefficients which completely specify the (small signal) microwave response of the hot-electron gas at an arbitrary frequency. This procedure will be described in detail elsewhere.[26]

ACKNOWLEDGMENT

It is a pleasure to thank N. I. Meyer, K. V. Hansen, and B. Vinter for valuable discussions.

APPENDIX A: NUMERICAL SOLUTION OF THE BOLTZMANN EQUATION

We shall indicate how Eqs. (6)–(8) are solved to obtain $\vec{G}_\nu$ (which is all we need to calculate the current contributions from the different valleys).

Introducing the functions:

$$\begin{aligned} y_\nu(K) &= K^2 F_\nu(K)\,, \\ \vec{g}_\nu(K) &= K^4 \vec{G}(K)\,, \\ \vec{h}_\nu(K) &= K^5 \dot{\vec{K}}_\nu \cdot \vec{\vec{H}}_\nu(K)\,, \end{aligned} \tag{A1}$$

and using the relaxation-time approximations (12) and (13), we may write (6)–(8) in the form:

$$\left(\frac{\partial y_\nu}{\partial t}\right)_{\text{scatt}} - \frac{1}{3}\frac{\partial}{\partial K}\left(\frac{1}{K}\dot{\vec{K}}_\nu \cdot \vec{g}_\nu\right) = 0\,, \tag{A2}$$

$$\vec{\tau}_\nu^{-1} \cdot \vec{g}_\nu - \dot{\vec{K}}_\nu\left(2y_\nu - K\frac{\partial}{\partial K}y_\nu\right) + \frac{2}{5}\frac{\partial}{\partial K}\vec{h}_\nu = 0\,, \tag{A3}$$

$$\frac{1}{\tau_{\nu\perp}}\vec{h}_\nu + \tfrac{1}{2}K^4\frac{\partial}{\partial K}\left(\frac{1}{K^4}\left(\dot{\vec{K}}_\nu^2\vec{\vec{1}} + \tfrac{1}{3}\dot{\vec{K}}_\nu\dot{\vec{K}}_\nu\right)\cdot\vec{g}_\nu\right) = 0\,. \tag{A4}$$

Assuming weak scattering anisotropy, we can simplify the calculation of the higher-order term $\vec{h}_\nu$ by assuming $\vec{g}_\nu$ and $\dot{\vec{K}}_\nu$ to be parallel. Then Eq. (A4) gives

$$\vec{h}_\nu \simeq \Phi_\nu(K)\left(4\vec{g}_\nu - K\frac{\partial}{\partial K}\vec{g}_\nu\right)\,, \tag{A5}$$

with

$$\Phi_\nu(K) \equiv 2\dot{\vec{K}}_\nu^2\tau_{\nu\perp}/3K\,. \tag{A6}$$

Inserting (A5) into (A3) we get

$$\left\{\frac{2}{5}\left[K\Phi_\nu\frac{\partial^2}{\partial K^2} + \left(K\frac{\partial\Phi}{\partial K} - 3\Phi_\nu\right)\frac{\partial}{\partial K} - 4\frac{\partial\Phi_\nu}{\partial K}\right]\vec{\vec{1}} - \vec{\tau}_\nu^{-1}\right\}\cdot\vec{g}_\nu = \dot{\vec{K}}_\nu\left(K\frac{\partial}{\partial K} - 2\right)y_\nu\,. \tag{A7}$$

We may interprete (A7) as a set of 3 (mutally independent) ordinary second-order differential equations which may be solved for $\vec{g}(K)$ when $y(K)$ is known. Because of the axial symmetry of the conduction band valleys we only need to solve two of these equations to find $g_{\nu\perp}$ and $g_{\nu\parallel}$. The particular solutions to be used are identified by the boundary conditions $\vec{g}_\nu(K) \to 0$ for $K \to 0$ and $K \to \infty$.

If the $\vec{h}_\nu$ term in (A3) is neglected (as in the usual "diffusion approximation") all terms with Φ_ν vanish from (A7) and we get the simple solution:

$$\vec{g}_\nu^{\,0}(K) = \vec{\tau}_\nu \cdot \dot{\vec{K}}_\nu\left(2 - K\frac{\partial}{\partial K}\right)y_\nu(K)\,,$$

which eventually turns out to be a useful trial function. Finally the expression (20) for $(\partial F_\nu/\partial t)_{\text{scatt}}$ is used and (A2) may now be written:

$$\begin{aligned} &\tfrac{1}{2}W_{ace}kT\frac{d}{dK}\left\{[K\zeta(K)]^2\left[\frac{\zeta(K)}{2K}\frac{\partial y_\nu}{\partial K} + \left(\frac{1}{kT} - \frac{\zeta(K)}{K^2}\right)y_\nu\right]\right\} - \frac{1}{3}\frac{\partial}{\partial K}\left[\frac{1}{K}\dot{\vec{K}}_\nu\cdot\vec{\tau}_\nu\cdot\dot{\vec{K}}_\nu\left(2 - K\frac{\partial}{\partial K}\right)y_\nu\right] \\ &\quad - \sum_{\mu\neq\nu}\sum_m W_{\mu\nu}^{(m)}\left[K_-\zeta(K_-)(n_{\mu\nu}^{(m)}+1) + K_+\zeta(K_+)n_{\mu\nu}^{(m)}\right]y_\nu \\ &\quad = -\sum_{\mu\neq\nu}\sum_m W_{\mu\nu}^{(m)}K^2\left[\zeta(K_-)y_\mu(K_-)n_{\mu\nu}^{(m)}/K_- + \zeta(K_+)y_\mu(K_+)(n_{\mu\nu}^{(m)}+1)/K_+\right] + \frac{1}{3}\frac{\partial}{\partial K}\left(\frac{1}{K}\dot{\vec{K}}_\nu\cdot\delta\vec{g}_\nu\right)\,. \end{aligned} \tag{A8}$$

Here $K_\pm$ is defined in Eq. (19), and

$$\delta\vec{g}_\nu(K) \equiv \vec{g}_\nu(K) - \vec{g}^0_\nu(K). \quad \text{(A9)}$$

The $\delta\vec{g}_\nu$ term on the right-hand side of (A8) is necessary because the trial function $\vec{g}^0_\nu(K)$ has been inserted into the field term on the left-hand side instead of the proper function $\vec{g}(K)$. This is done in order to facilitate an iterative solution of (A8). For the same reason the intervalley phonon scattering term has been split such that "scattering into state $\vec{K}$" is moved to the right-hand side and "scattering out of state $\vec{K}$" is retained on the left-hand side of Eq. (A8) (together with the acoustic-phonon scattering term). If the right-hand side of Eq. (A8) is a known function of K, the problem is reduced to the solution of an ordinary second-order differential equation [with boundary conditions $y_\nu(K) \to 0$ for $K \to 0$ and $K \to \infty$].

The initial step in the iterative procedure is the (rather uncritical) choice of trial functions for $y_\nu(K)$ and $\delta\vec{g}_\nu(K)$. Then the iterative procedure is entered: (i) The function on the right-hand side of Eq. (A8) is calculated from $y_\nu(K)$ and $\delta\vec{g}_\nu(K)$. (ii) An improved version of $y_\nu(K)$ is now obtained by solving (A8) as a differential equation with respect to the y_ν function appearing on the left-hand side. (iii) Using the improved version of $y_\nu(K)$ the differential equations in (A7) are solved to obtain improved versions of $\vec{g}_\nu(K)$ [and $\delta\vec{g}_\nu(K)$]. (iv) The whole sequence [beginning with step (i)] is repeated until the correction to $y_\nu(K)$ made in each cycle is approaching zero. From the finally accepted version of $y_\nu(K)$ the valley population factors and the "electron temperatures" are calculated and, more important, the final version of $\vec{g}_\nu(K)$ which determines the average electronic drift velocity.

To summarize, we have shown that in the "extended diffusion approximation" the Boltzmann equation for n-Si may be solved by carrying out a limited number of iterative cycles. In each cycle a set of independent, ordinary second-order differential equations must be solved with fixed boundary conditions. In principle, this set contains 6 $y_\nu(K)$ equations and 18 $\vec{g}_\nu(K)$ equations. However, one may take advantage of the conduction-band symmetries and solve only 3 $y_\nu(K)$ equations and 6 $\vec{g}_\nu(K)$ equations in the general case. (A further reduction is possible if the electric field as well as the axis of a possible uniaxial pressure are parallel to one of the ⟨111⟩, ⟨110⟩, or ⟨100⟩ directions.)

With typical n-Si parameters one calculation with an overall accuracy of 0.5% (on the y_ν functions) will require 4 to 12 iterative cycles (less than 2 sec central-processor unit time on an IBM 370/165).

The accuracy of the extended diffusion approximation has been tested by comparison with accurate Monte Carlo calculations (with less than 5% statistical error on the drift velocity). At high electric fields the results are identical (whereas the ordinary diffusion approximation without "streaming" corrections gives drift velocities which are typically 10% too high). At lower electric fields the number of free flights required for an accurate Monte Carlo calculation becomes prohibitively large. Even at high fields, however, iterative solutions are more than ten times faster than Monte Carlo simulations.

If at least 15 iterative cycles are allowed the accuracy at lower electric fields (in the warm-electron region) becomes sufficiently high for a determination of the warm electron coefficients[3] β and γ. In this case one must define a function $\beta(E)$ by $v_d(E) = \mu(0)[E + E^3\beta(E)]$. After calculating $\beta(E)$ for a few properly chosen field-values the "true" β-coefficient $\beta(0)$ can be found by extrapolation since $\beta(E)$ varies linearly with E^2 at low electric fields. Similar techniques apply to the coefficient γ which describes the transverse anisotropy in the warm electron range.[3]

Finally, it is worth mentioning that the "streaming" of the electronic distribution (as described by $\vec{h}_\nu$ or $\vec{H}_\nu$) is not a specific high field or "hot-electron" effect but should, in principle, be included as soon as *any* nonlinear transport effect is considered. In our calculations typical deviations of (10–15)% are found when $\vec{h}_\nu$ terms are left out in β calculations.

TABLE III. Acoustic-phonon coefficients.

i	$A_{i\perp}$	$A_{i\parallel}$	A_{i0}
1	1.04	1.58	1.57
2	1.14	2.46	3.13
3	1.34	1.40	2.23
4	0.85	2.48	2.58
5	0.73	1.10	1.29
6	1.70	2.25	3.16

APPENDIX B: SCATTERING COEFFICIENTS USED IN NUMERICAL CALCULATIONS

The effective deformation potentials $\Xi_\perp$, $\Xi_\parallel$, and Ξ_0 appearing in Eqs. (15) and (21) are defined by

TABLE IV. Impurity scattering coefficients.

λ	a_λ	b_λ	c_λ	d_λ
$\perp$	3.765	0.788	1.384	5.87
$\parallel$	1.059	1.226	1.133	4.97

$$\Xi_\lambda^2 = \Xi_u^2[A_{1\lambda} + (A_{2\lambda} + BA_{3\lambda})B + (A_{4\lambda} + CA_{5\lambda} + BA_{6\lambda})C] \quad \text{(B1)}$$

with $\lambda = \perp$, $\parallel$ or 0. The constants B and C are defined by

$$B = (\Xi_d + C_1)/\Xi_u \text{ and } C = C_2/\Xi_u . \quad \text{(B2)}$$

The coefficients $A_{i\lambda}$ are listed in Table III.

A detailed discussion of the $A_{i\perp}$ and $A_{i\parallel}$ coefficients is found in Ref. [2]. The impurity scattering coefficients $a_\lambda, \ldots, d_\lambda$ appearing in Eq. (14) are given in Table IV for n-Si.

[1] C. Herring and E. Vogt, Phys. Rev. 101, 944 (1956).
[2] N. O. Gram and M. H. Jørgensen, Phys. Rev. B 8, 3902 (1973).
[3] M. H. Jørgensen, Phys. Rev. 156, 834 (1967).
[4] H. G. Reik and H. Risken, Phys. Rev. 124, 777 (1961).
[5] I. Balslev, Phys. Rev. 143, 636 (1966).
[6] D. Long, Phys. Rev. 120, 2024 (1960).
[7] P. Norton, T. Braggins and H. Levinstein, Phys. Rev. B 8, 5633 (1973).
[8] M. Asche, V. M. Vasetsky, A. G. Maximchuk, and O. G. Sarbey, Ukr. Fiz. Zh. 15, 1692 (1970).
[9] A. J. Pindor, J. Phys. C 5, 2357 (1972).
[10] H. W. Streitwolf, Phys. Status Solidi 37, K47 (1970).
[11] H. W. Streitwolf, *Gruppentheorie in der Festkörperphysik* (Geest and Portig, Leipzig, 1967).
[12] M. Lax and J. J. Hopfield, Phys. Rev. 124, 115 (1961).
[13] G. Dolling, *Symposium on Inelastic Scattering of Neutrons in Solids and Liquids* (IAEA, Vienna, 1963), Vol. II, p. 37.
[14] L. Eaves, R. A. Hoult, R. A. Stradling, R. J. Tidey, J. C. Portal, and S. Askenazy, J. Phys. C 8, 1034 (1975).
[15] K. V. Hansen, thesis (Tech. University of Denmark, Physics Lab. III, 1974) (unpublished).
[16] C. B. Norris and J. F. Gibbons, IEEE Trans. ED-14, 38 (1967).
[17] C. Canali, G. Majni, R. Minder, and G. Ottaviani: Electron. Lett. 10, 523 (1974).
[18] C. Jacoboni, R. Minder, and G. Majni, J. Phys. Chem. Solids 36, 1129 (1975).
[19] J. C. Ousset, J. Leotin, S. Askenazy, M. S. Skolnick, and R. A. Stradling, J. Phys. C 9, 2803 (1976).
[20] M. H. Jørgensen and N. I. Meyer, Solid State Commun. 3, 311 (1965).
[21] M.H. Jørgensen, thesis (Tech. University of Denmark, Physics Lab III, 1966) (in Danish) (unpublished).
[22] C. Canali, G. Ottaviani, and A. Alberigi Quaranta, J. Phys. Chem. Solids 32, 1707 (1971).
[23] W. Sasaki and M. Shibuya, J. Phys. Soc. Jpn. 11, 1202 (1956).
[24] K. J. Schmidt-Tiedemann, Phys. Rev. 123, 1999 (1961).
[25] E. M. Conwell, *High Field Transport in Semiconductors* (Academic, New York, 1967).
[26] M. H. Jørgensen (unpublished).